Temperature dependence of magnetoresistance and Hall effect in Mg_2NiH_x films

S. Enache, W. Lohstroh, and R. Griessen
Faculty of Sciences, Department of Physics and Astronomy, Condensed Matter Physics, Vrije Universiteit, De Boelelaan 1081, 1081 HV Amsterdam, The Netherlands

(Received 14 October 2003; published 22 March 2004)

The electrical resistivity, Hall effect, and magnetoresistance of Mg_2NiH_x ($0<x<4$) films are investigated as a function of temperature, between 2 K and 280 K and magnetic fields up to 7 T. The overall features exhibited by the electrical resistivity ρ and the charge-carrier density n at 4.2 K in $Mg_2NiH_{4-\delta}$ are those of a heavily doped semiconductor. As a function of x, accompanied by an increase of ρ, n decreases linearly. This is consistent with an ''anionic'' model for H in the host lattice: each added H atom removes one electron from the conduction band, resulting in an increased resistivity. Over the entire concentration range (for $0<x<4$), we find approximately that $\rho(T)\simeq\rho_0-\rho_1\ln T+\rho_2T^{1.85}$. The amplitude ρ_1 of the Kondo term and ρ_2 of the electron-electron scattering term vary by more than two orders of magnitude and exhibit power-law dependence as a function of n. The experimental data can be understood within an effective medium theory, where Mg_2NiH_x samples disproportionate into metallic $Mg_2NiH_{0.3}$ and semiconducting $Mg_2NiH_{4-\delta}$. In this picture, we show that the relatively low ρ ($<4\text{m}\Omega$ cm) measured in samples with $x\lesssim3.5$ is due to the peculiar geometry of the metallic inclusions (very flat oblate spheroids). The relation with the highly absorbing black state in $Mg_2NiH_{0.7}$ is discussed.

DOI: 10.1103/PhysRevB.69.115326 PACS number(s): 73.43.Qt, 73.50.−h, 78.40.Fy, 77.84.Lf

I. INTRODUCTION

In 1996, Huiberts *et al.*[1] discovered that palladium capped yttrium and lanthanum films switch reversibly and rapidly between a shiny metal and a transparent insulator upon hydrogen absorption. Since then, other rare-earth hydrides[2] (REH_x) and some of their alloys[3] were shown to exhibit similar switching properties. In a search for wide-band-gap switchable mirrors, Van der Sluis *et al.*[2] discovered the color neutral Mg-alloyed REH_x hydrides. Recently, the class of switchable mirrors was extended to rare-earth free intermetallic compounds, when Richardson *et al.*[4] reported that thin films of Mg_2Ni exhibit switchable mirror behavior.

Bulk intermetallic Mg_2Ni can dissolve H in solid solution up to $Mg_2NiH_{0.3}$. Upon further H absorption, the system undergoes a structural rearrangement to the stoichiometric Mg_2NiH_4 hydride,[5] with an accompanying 32% increase in volume.[6] This hydride is the only stable ternary compound known for the Mg-Ni-H system. Because of its relative low weight and high hydrogen content, Mg_2NiH_4 has been extensively studied for hydrogen storage purposes.

Above 510 K, bulk Mg_2NiH_4 transforms to a high-temperature (HT) cubic phase, where the metal atoms are arranged in an antifluorite-type structure.[7] The low-temperature (LT) phase is monoclinic, but it can be visualized as a slightly distorted antifluorite lattice.[8]

For the HT-Mg_2NiH_4 phase, the hydrogen atomic positions have been investigated experimentally by neutron-diffraction techniques.[9,10] The data indicate that the four H atoms are positioned around Ni ($d_{Ni\text{-}H}=1.55$ Å), rather than in the neighborhood of Mg ($d_{Mg\text{-}H}=2.07$ Å). Therefore, the Mg_2NiH_4 system may be considered as a complex metal-hydride formed of $[NiH_4]^{4-}$ complexes and Mg^{2+} ions.

Using *ab initio* total-energy calculation, Garcia *et al.*[11] showed that the ground state of the HT-Mg_2NiH_4 phase depends crucially on the spatial configuration of the four H atoms in the $[NiH_4]^{4-}$ complex. For a square planar, a distorted, or a regular tetrahedral configuration of the H atoms within a given $[NiH_4]^{4-}$ complex, the ground state is, respectively, metallic, semi-metallic, or semiconducting with an indirect band gap $E_g=1.14$ eV. For the LT-Mg_2NiH_4 phase with a nearly undistorted tetrahedral hydrogen configuration, Myers *et al.*[12] obtained a semiconductor with an indirect band gap of $E_g=1.4$ eV. The overall features of the electronic structure of the LT phase resemble those of the semiconducting HT phase found by Garcia *et al.*[11] The ground states of these systems are determined mainly by the spatial configuration of individual $[NiH_4]^{4-}$ complexes. This has been explicitly demonstrated by Garcia *et al.*[11] with a band-structure calculation of a hypothetical Mg_2NiH_4 compound in which the Mg atoms had been removed. Therefore, the principal role of Mg is to stabilize the crystal structure of the compound and to donate its two valence electrons.

As far as we know, there are only a few investigations of the electrical transport properties of bulk $Mg_2NiH_{4-\delta}$.[13,14] For instance, in compressed powders of the LT-$Mg_2NiH_{4-\delta}$ phase prepared at H_2 pressures between 0.02 and 10 kbar, Blomqvist and Noreus[14] found that the electrical resistivity is fairly low and depends hardly on temperature (above 110 K). These features led Blomqvist and Noreus to the conclusion that the LT-$Mg_2NiH_{4-\delta}$ phase is a heavily doped semiconductor, as a result of nonstoichiometry and, probably, uncontrolled doping during sample preparation.

Electrical-transport measurements on Mg_2NiH_4 powders are tricky to interpret. This is the reason why films of intermetallic Mg_2Ni alloy are investigated in this work, since they absorb hydrogen readily and without embrittlement at moderate pressures (below 1 bar H_2) to form $Mg_2NiH_{4-\delta}$.[4] Therefore, the possibility to synthesize Mg_2NiH_x films offers a unique opportunity to investigate in detail their intrinsic physical properties as a function of H concentration. At room

temperature, these films exhibit large changes in their electrical and optical properties, as they switch from shiny metallic Mg_2Ni to transparent and semiconducting $Mg_2NiH_{4-\delta}$ upon H absorption.[4,15]. At low H concentrations ($0<x<0.7$), although these films are metallic (with relatively low resistivity $\rho<100\mu\Omega$cm) and nontransparent, they exhibit unusually high optical absorption. Their optical reflection is less than 15% over the entire visible spectrum, while the optical transmission is extremely low ($<0.01\%$).[15] From a simple Drude analysis of reflectance spectra (the transmission being so small that it could not be measured), Isidorsson *et al*. concluded that an unusually large decrease (by a factor 25) of the charge-carrier density might be the cause of the highly absorbing state in $Mg_2NiH_{0.7}$. As such a large effect could not be understood within a rigid-band model, it was suggested that a Peierls transition[15] was operative.

In this paper, in order to shed more light on the occurrence of the highly absorbing state and the metal-to-semiconductor transition in Mg_2NiH_x films, we investigate in detail the temperature dependence of the electrical resistivity, Hall effect, and magnetoresistance for x between 0 and 4.

The overall features exhibited by the electrical resistivity ρ and the charge-carrier density n in Mg_2NiH_x (for $0<x<4$) are consistent with the ''anionic'' model of H in the host lattice: each H atom removes one electron from the conduction band to form a negative H^- ion. Upon H absorption, n decreases gradually while ρ increases and diverges for nearly stoichiometric $Mg_2NiH_{4-\delta}$. At low temperatures ($T<10$ K), we find that $\rho(T)\propto-\ln T$, which points to a Kondo effect.[16] At intermediate temperatures ($25\text{ K}<T<80$ K), $\rho(T)\sim T^{\alpha}$, where $\alpha=(1.85\pm0.30)$. This may be due to electron-electron scattering effects.[17] The intriguing aspect of these dependencies is that they hold for samples with ρ differing by more than two orders of magnitude.

The electrical and magnetotransport data are analyzed in the framework of an effective medium theory,[18] where Mg_2NiH_x samples with $0.3<x<4$ disproportionate into metallic $Mg_2NiH_{0.3}$ and semiconducting $Mg_2NiH_{4-\delta}$. Experimental data on the low-temperature resistivity $\rho(T=1\text{ K})$, the amplitude of the Kondo and electron-electron scattering terms as a function of the charge-carrier density obtained from Hall-effect measurements at 4.2 K, are used to determine the geometry of the constitutive inclusions.

Finally, we compare our electrical and magnetotransport data with those obtained in the $Sc_{1-y}Ti_yN$ systems.[19] These alloys are somewhat similar to Mg_2NiH_x. For instance, gradual substitution of Ti by Sc drives $Sc_{1-y}Ti_yN$ from metallic (TiN) to semiconducting (ScN). Some particularities of the optical and electrical transport properties of these systems are discussed.

II. EXPERIMENT

Thin films of Mg_2Ni are prepared by sputtering. A description of the deposition conditions is reported elsewhere.[15] Glassy carbon and Corning 7059 substrates are used for Rutherford backscattering spectrometry (RBS) and electrical measurements, respectively. The films are covered *in situ* with a thin layer (~2 nm) of Pd to protect them against oxidation and to promote H dissociation and absorption. The composition and film thickness (~232 nm) are determined *ex situ* by means of RBS. The Mg:Ni atomic ratio is 2.17:1. Contamination with O (up to 8.2% per Mg atom) is observed in RBS spectra at the interface with the substrate, which most probably is bound in the form of complex MgO_x oxides. The x-ray spectra indicate that our films are nanocrystalline with coherence length of ~30 nm.

Electrical resistivity, magnetoresistance and Hall-effect measurements are carried out using the van der Pauw method.[20] For that, four Au leads (25 μm in diameter) are connected by ultrasonic wedge bonding at the edge of the sample in a squarelike pattern. Two Stanford research instruments (models 830 and 850) equipped with vector lock-in amplifiers and variable ac-power supplies are connected in a typical lock-in electrical circuit including an external 10 kΩ variable resistance in series with the sample via a Keithley 7001 Multiplexer. The lock-in frequency is 113 Hz. The applied current on the sample ranges between 10 μA and 1 mA. For Hall measurements, the voltage *perpendicular* to the current is measured for positive and negative magnetic fields. The data are corrected for magnetoresistance contributions due to misalignment of the voltage probes. The effective charge-carrier density n is calculated according to

$$n=\frac{I}{d|e|}\frac{B}{V_H}, \tag{1}$$

where d is the sample thickness (~232 nm), $|e|$ is the elementary charge ($\sim1.60\times10^{-19}$ C), and V_H is the Hall voltage measured at current I in magnetic field B. For magnetoresistance (MR) measurements, the voltage *parallel* to the current is collected for both directions of the magnetic field, and the residual Hall contribution to the MR signal is subtracted. The magnetoresistance MR is calculated from

$$\text{MR}=\frac{\rho(B)-\rho(0)}{\rho(0)}, \tag{2}$$

where $\rho(B)$ is the electrical resistivity in the external magnetic field B, while $\rho(0)$ is the electrical resistivity in zero field.

The low-temperature (2 K–250 K) electrical and magnetotransport measurements are performed in a He-bath cryostat from Oxford Cryogenics Instruments equipped with a 7 T superconducting magnet. Temperature is swept at a rate slower than 0.3 K/min during which the electrical resistivity is measured continuously. The MR and Hall measurements are carried out at constant temperature during the cooling procedure. Temperature stability during these measurements is better than 0.05 K. The temperature is monitored continuously with a hydrogen insensitive Lake Shore Rh-Fe-100 resistor, which is mounted close to the sample.

Various H concentrations in Mg_2NiH_x are prepared at room temperature in gaseous H_2 at pressures between 5 and 1300 mbar. Samples with low concentrations ($0<x<0.7$) are prepared in an optical loading cell. Upon H loading, the reflection is monitored so as to carefully tune the sample in its highly absorbing state. Samples with $0.7<x<4$ are prepared in the sample chamber of the cryostat in connection

with a vacuum cell. The sample is then cooled in H_2 atmosphere down to ~ 20 K. In order to achieve temperatures as low as to 4.2 K, He gas is added (at $T \simeq 20$ K). To check the ohmic contacts, *I-V* characteristics (1 μA–10 mA) and frequency dependent signals (50 Hz–15 kHz) were recorded at 200 K. Also, in order to check that the distribution of H in the sample is homogeneous, the electrical resistivity is measured in two distinct van der Pauw configurations.

Due to a large volume expansion occurring in Mg_2NiH_x hydrides upon hydrogen absorption (up to $\sim 32\%$ at $x=4$),[6] the measured electrical resistivity and Hall-effect data need to be corrected for an increase in thickness of our films. For that, we assume that the relative volume increase $\varepsilon(x) = \Delta V(x)/V_0$ in Mg_2NiH_x with respect to that in Mg_2Ni occurs mainly *out of plane* of the film, since these films are rigidly clamped to the substrate. As $\varepsilon(x) = \Delta V(x)/V_0 = 0.08x$ for $0 < x < 4$,[21] the *real* thickness of the Mg_2NiH_x film is $d(x) = [1+\varepsilon(x)]d_0$, where $d_0 = 232$ nm is the thickness of the as-deposited Mg_2Ni film. Note that some physical quantities defined at fixed concentration x, which involve products or ratios between the electrical resistivity and the Hall-effect data [such as MR defined in Eq. (2), the scattering time $\tau \propto R/\rho = e/n\rho$, etc.], are not affected by this correction.

III. EXPERIMENTAL RESULTS

In this section, we present experimental data concerning the electrical resistivity, Hall effect, and magnetoresistance of our Mg_2NiH_x films as a function of H concentration and temperature.

At 295 K, the as-prepared 232 nm thick Mg_2Ni films are metallic and characterized by a relatively *low* electrical resistivity ($\rho_{295\,K} = 55.1$ $\mu\Omega$cm) and a *high* effective charge-carrier density ($n_{295\,K} = 7.35 \times 10^{22}$ cm^{-3}). At 4.2 K, the residual resistivity value is 47.2$\mu\Omega$cm. The residual resistivity ratio is poor ($\rho_{295\,K}/\rho_{4.2\,K} \sim 1.16$). The effective charge-carrier density at 4.2 K is 8.65×10^{22} cm^{-3}. This value is ~ 1.17 times higher than that at 295 K.

In Fig. 1, n in Mg_2NiH_x determined from Hall-effect measurements at 4.2 K drops by approximately two orders of magnitude, from 8.65×10^{22} cm^{-3} in metallic Mg_2Ni to 9.28×10^{20} cm^{-3} for $Mg_2NiH_{4-\delta}$. Thus at the maximum H concentration reached in this work, n is still high and does not significantly depend on temperature. The drop of n is accompanied by a large increase of the electrical resistivity ρ (see Fig. 2) well over two orders of magnitude, from 47.2 $\mu\Omega$cm in metallic Mg_2Ni to 12.9 mΩcm for $Mg_2NiH_{4-\delta}$. *Qualitatively*, these features resemble those reported by Blomqvist and Noreus in compressed powders,[14] but *quantitatively*, our Mg_2NiH_x films have a much lower resistivity. This is not surprising as electrical measurements on compressed powders are strongly influenced by intergrain resistivities. From the overall features of ρ and n, we conclude that $Mg_2NiH_{4-\delta}$ is a heavily doped semiconductor.

Let us now comment on the features exhibited by n and ρ at low hydrogen concentrations (that is, for $0 < x < 0.7$ in Figs. 1 and 2, respectively), corresponding to the occurrence of the highly absorbing state discovered by Isidorsson *et al.*[15]

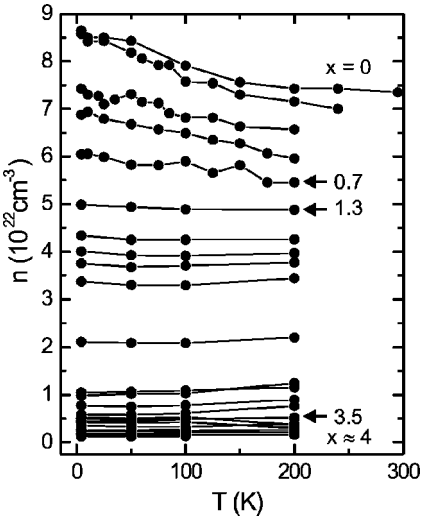

FIG. 1. Charge-carrier density n as a function of temperature in Mg_2NiH_x (with $0 < x < 4$). The curves corresponding to Mg_2NiH_x samples with concentrations $x \simeq 0$, 0.7, 1.3, 3.5, and ≈ 4 are indicated explicitly.

in metallic films (with $\rho < 100$ $\mu\Omega$cm). In the first report,[15] it was suggested that the black state occurs at $x \sim 0.3$. However, Lohstroh *et al.*[22] have accumulated ample experimental evidence that the highly absorbing state is fully developed at slightly higher concentrations (at $x \sim 0.7$). We find here that the electrical properties of black $Mg_2NiH_{0.7}$ are essentially similar to those reported in Ref. 15; i.e., these samples are highly conducting ($\rho < 100$ $\mu\Omega$cm) and nontransparent, with optical reflection less than 15% over the entire visible spectrum. This is shown in Fig. 2, where ρ at 4.2 K increases by a factor of ~ 1.8, from 47.2 $\mu\Omega$cm in shiny metallic Mg_2Ni to 84.6 $\mu\Omega$cm for black $Mg_2NiH_{0.7}$. On the other

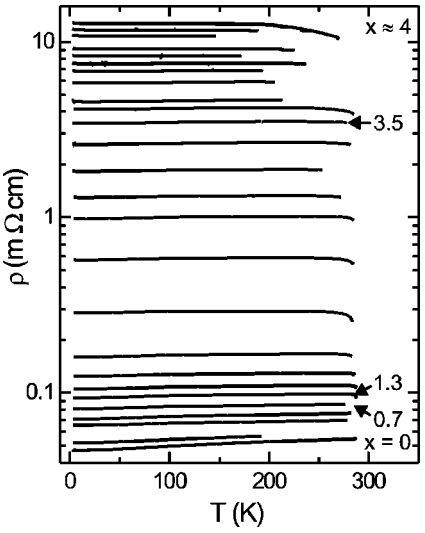

FIG. 2. Electrical resistivity ρ as a function of temperature in Mg_2NiH_x ($0 < x < 4$). The curves corresponding to Mg_2NiH_x samples with concentrations $x = 0$, 0.7, 1.3, 3.5, and ≈ 4 are indicated explicitly. The decreasing electrical resistivity above 220 K is due to hydrogen loss in the sample.

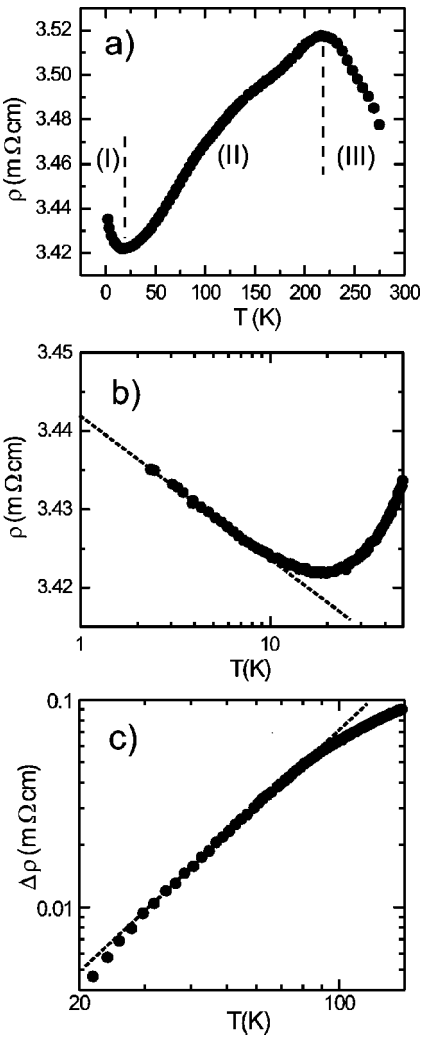

FIG. 3. Temperature dependence of the electrical resistivity ρ of $Mg_2NiH_{\simeq 3.5}$ over the whole temperature range (a). Below 10 K (b) the data follow a logarithmic temperature dependence $\rho(T) \simeq \rho_0 - \rho_1 \ln T$. At intermediate temperatures (c), the difference $\Delta\rho(T) = \rho(T) - \rho_0 + \rho_1 \ln T$ is power law up to $\simeq 80$ K, i.e., $\Delta\rho(T) \simeq \rho_2 T^{\alpha}$. The values of $\rho(T)$ are taken from (a) and those of ρ_0 and ρ_1 from (b).

hand, n obtained from Hall-effect data at 4.2 K (see in Fig. 1) drops only by a factor ~ 1.43 with increasing x, from 8.65×10^{22} cm^{-3} in metallic Mg_2Ni to nearly 6.05×10^{22} cm^{-3} for black $Mg_2NiH_{0.7}$. These data do not support the large drop in charge-carrier density in Ref. 15, i.e., there is no dramatic reduction on n (by a factor 25) at the transition from metallic Mg_2Ni to black $Mg_2NiH_{0.7}$.

So far we have only looked at the gross features exhibited by ρ and n as a function of x. However, although the electrical resistivity curves in Fig. 2 are constant within a few percents, they exhibit several general characteristic features as a function of T. As a typical example, we consider the results for the Mg_2NiH_x sample with $x \sim 3.5$ [see in Fig. 3(a)]. With respect to the sign of the temperature derivative of ρ (i.e., $d\rho/dT$), three conduction regimes are distinguished. At high temperatures, in regime (III), the electrical resistivity increases with decreasing temperature ($d\rho/dT < 0$). This is due to absorption of H by the sample during cooling in H_2 atmosphere. This temperature activated process is possible down to ~ 220 K. Below 220 K, further absorption of H is hampered by the slow kinetics and therefore, the H concentration in the film remains constant. At intermediate temperatures, in regime (II), $\rho(T)$ exhibits metalliclike behavior with a positive $d\rho/dT$. This holds down to $T_{min} \sim 18.3$ K, where the electrical resistivity goes through a minimum. Below $T_{min} \sim 18.3$ K, in regime (I), $d\rho/dT < 0$.

In the low-temperature regime (I), various functional forms usually used to describe $\rho(T)$ in semiconductors (such as thermal activation and variable range hopping[23]) do not fit our experimental results. Below 10 K, we find instead a *logarithmic* $\rho(T)$ dependence [see in Fig. 3(b)]. This suggests an interpretation in terms of Kondo scattering of the free electrons on localized magnetic impurities.[16] The magnetic impurities are probably Ni clusters or atoms that have not reacted with Mg to form Mg_2Ni.

For the analysis of our measurements we use the following expression:

$$\rho(T) = \rho_0 - \rho_1 \ln T + \rho_2 T^{\alpha}. \tag{3}$$

The Kondo term (i.e., $-\rho_1 \ln T$) is important at low temperatures (below 10 K). The power-law term $\rho_2 T^{\alpha}$ is the contribution to ρ from electron-phonon or electron-electron scattering processes. For electron-phonon scattering, the power-law term scales as T (with $\alpha = 1$) at high temperatures and as T^5 (with $\alpha = 5$) at low temperatures.[24] Electron-electron scattering leads to a T^2 contribution to ρ.[17] It is well known that the presence of the power-law term in Eq. (3) is essential to reproduce the resistivity minimum observed in dilute magnetic alloys.[16]

In the fit of the $\rho(T)$ curve in Fig. 3(a), we focus first on the logarithmic dependence. In Fig. 3(b), the extrapolation of ρ at $T = 1$ K and the slope yields the values $\rho_0 \sim 3.44$ mΩcm and $\rho_1 \sim 8.25 \times 10^{-3}$ mΩcm, respectively. Subsequently, the Kondo contribution is subtracted from the $\rho(T)$ curve. In Fig. 3(c), we show that the remaining electrical resistivity $\Delta\rho(T) = \rho(T) - \rho_0 + \rho_1 \ln T$ exhibits power-law dependence over a wide temperature range (between 25 K and 80 K). A fit to $\Delta\rho(T)$ yields $\rho_2 \sim 3.47 \times 10^{-5}$ mΩ cm and $\alpha = (1.66 \pm 0.05)$.

The values obtained for the fit parameters in Eq. (3) lead also to the correct value for the temperature T_{min} corresponding to the resistivity minimum:

$$T_{\min} = (\rho_1 / \rho_2 \alpha)^{1/\alpha}. \tag{4}$$

Substituting the values obtained for ρ_1, ρ_2, and α in Eq. (4), we obtain $T_{min} \simeq 19.7$ K. This value agrees with the measured temperature (~ 18.3 K) corresponding to the minimum of the $\rho(T)$ curve shown in Fig. 3(a).

Although not directly visible because of the logarithmic scale used in Fig. 2, it turns out that *all* the electrical resistivity curves in this figure exhibit $\ln T$ dependence below 10 K and power law between 25 K $\lesssim T \lesssim$ 80 K. Therefore, *all* these curves can be analyzed as described above. The fitted values of ρ_0, ρ_1, ρ_2, α, and T_{min} for all these curves are

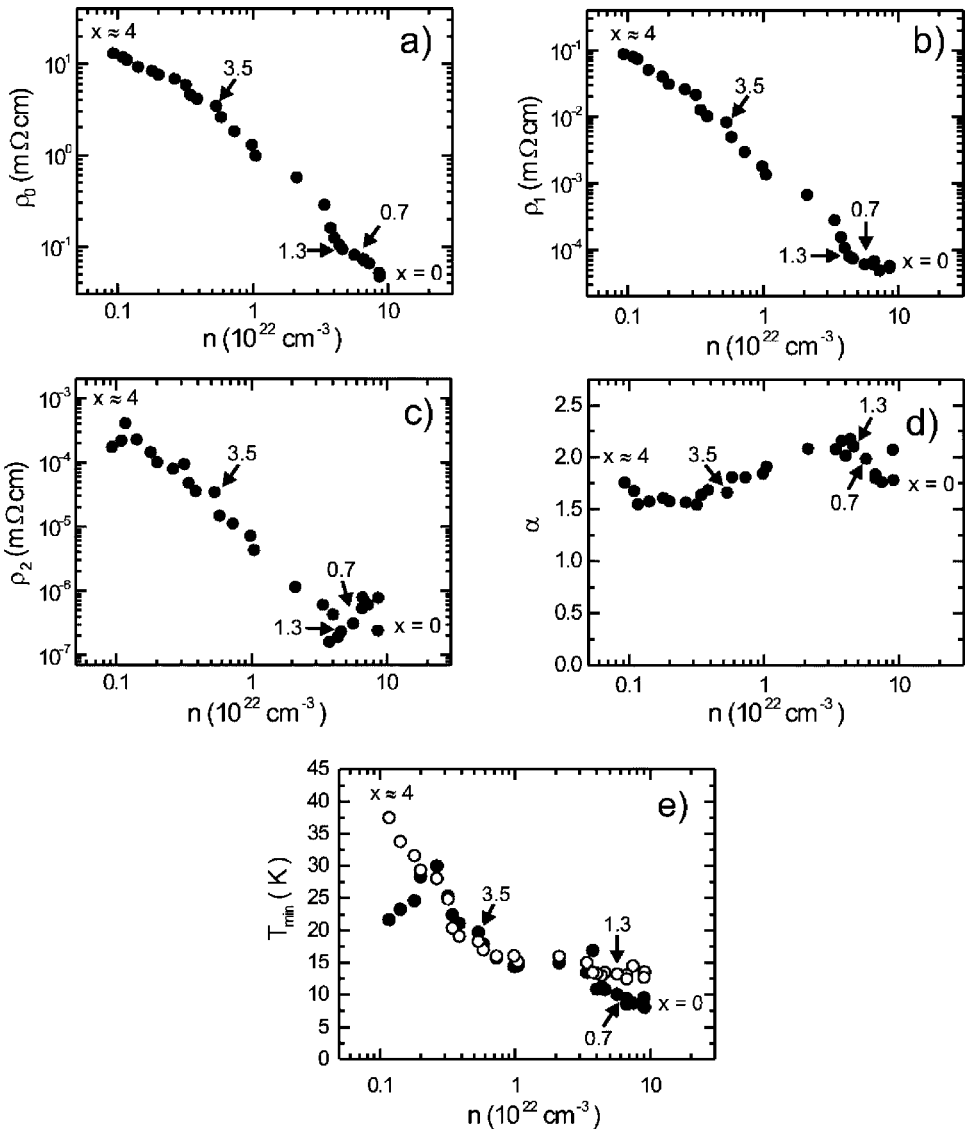

FIG. 4. Charge-carrier density dependencies of the electrical resistivity ρ_0 at $T=1$ K (a), the Kondo term ρ_1 (b), the electron-electron scattering term ρ_2 (c) and α involved in Eq. (3) (d). In panel (e) we compare the measured resistivity minima (bullets) with the calculated values T_{min} obtained from Eq. (4) (open symbols). The data corresponding to samples with $x \simeq 0$, 0.7, 1.3, 3.5, and ≈ 4 are indicated.

given in Figs. 4(a)–4(e) as a function of n obtained from Hall-effect measurements at 4.2 K. In Figs. 4(a)–4(c), the fit parameters ρ_0, ρ_1, and ρ_2 exhibit similar behavior with decreasing n (increasing x), in the sense that they increase well over two orders of magnitude as Mg_2NiH_x switches from metallic ($x=0$) to a semiconducting ($x\sim 4$). For some concentrations, the explicit dependence of these fit parameters as a function of n is power law. These power laws are summarized in Table I together with the concentration ranges for which they hold.

TABLE I. Power-law exponents β_i for the dependence of ρ_0, ρ_1, and ρ_2 on the charge-carrier concentration n obtained from Hall-effect data at 4.2 K. For $i=0$, 1, and 2, we assume $\rho_i \propto n^{-\beta_i}$.

Exponent	$0<x<0.7$	$0.7<x\lesssim 3.5$	$3.5\lesssim x<4$
β_0	0.93 ± 0.03	1.25 ± 0.02	0.69 ± 0.02
β_1		1.68 ± 0.03	0.69 ± 0.03
β_2		1.92 ± 0.05	1.92 ± 0.05

In Fig. 4(d), α is shown to be essentially independent of n. Its value (i.e., $\alpha=1.85\pm 0.30$) suggests that the contribution to the electrical resistivity due to electron-phonon scattering (with $\alpha=1$ and 5) is small and that electron-electron scattering effects (with $\alpha=2$, Ref. 17) prevail.

So far, using Eq. (3), we were able to determine the parameters ρ_0, ρ_1, ρ_2, and α. The values for T_{min} calculated using these parameters in Eq. (4) are in good agreement with the measured temperature minima [see Fig. 4(e)]. This implies that the temperature dependence of the electrical resistivity in our Mg_2NiH_x films (with $0<x<4$) is well described by Eq. (3).

In all samples ($0<x<4$), we find that the MR (7 T) (in 7 T field) is positive and extremely small (of the order of 10^{-5}–10^{-4}) at temperatures *above* T_{min}. However, as shown in Fig. 5, $MR_{4.2\,K}$ (7 T) obtained from measurements at 4.2 K is larger (of the order of 10^{-3}) and exhibits an interesting concentration dependence. At low H concentrations (for $0<x\lesssim 1.3$), $MR_{4.2\,K}$ (7 T) increases abruptly by a factor of ~ 1.5, from -10.6×10^{-4} in metallic Mg_2Ni to -7.3×10^{-4} for $Mg_2NiH_{1.3}$. In samples with $1.3\lesssim x\lesssim 3.5$,

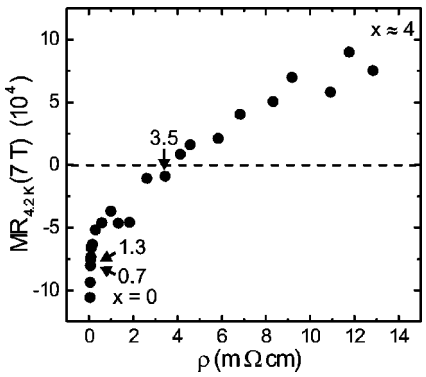

FIG. 5. Magnetoresistance $MR_{4.2\,K}$ (7 T) as a function of ρ in Mg_2NiH_x ($0<x<4$) obtained at 4.2 K in a magnetic field of 7 T. The data obtained in Mg_2NiH_x samples with $x \simeq 0$, 0.7, 1.3, 3.5, and $\simeq 4$ are indicated explicitly.

$MR_{4.2\,K}$ (7 T) decreases gradually to zero. Samples with $x \gtrsim 3.5$ exhibit positive $MR_{4.2\,K}$ (7 T) that increases steadily up to 9.8×10^{-4} for nearly stoichiometric $Mg_2NiH_{4-\delta}$.

IV. DISCUSSION

A. Model for H in the host lattice

The electrical and magnetotransport properties of our Mg_2NiH_x films ($0<x<4$) point towards an anionic picture for H in the host lattice: upon H absorption, electrons are gradually removed from the conduction band. This follows from the observed decrease of charge-carrier density n and the concomitant increase of the electrical resistivity, which diverges in nearly stoichiometric $Mg_2NiH_{4-\delta}$ samples. For a more quantitative discussion, it is, however, highly desirable to know the explicit relation between the charge-carrier density n and the H concentration x. For that purpose, electrochemical loading experiments in a standard three-electrode setup with a Hg/HgO reference electrode and a Pt counter electrode were performed. Simultaneously the optical reflection and transmission of the sample at the fixed wavelength $\lambda = 635$ nm are measured. Details are given by Lohstroh *et al.*[22] Since the optical properties exhibit some pronounced features [e.g., highly reflecting ground state followed by a sharp drop of the reflection with increasing H concentration and, subsequently, the onset of a weak optical transmission (see in Ref. 15)], the hydrogen concentration for these characteristic states can be determined. These results can directly be correlated to the data obtained from gas loading experiments in an optical spectrometer, where the electrical resistivity is measured simultaneously with the optical reflectance and transmission. In this way we are able to associate a hydrogen concentration to six different loading states of Mg_2NiH_x in Figs. 1 and 2. Unfortunately, a direct resistivity measurement during the electrochemical loading is not possible since homogeneous electrochemical loading is only possible for Mg_2Ni films deposited on conducting indium-tin-oxide substrates.

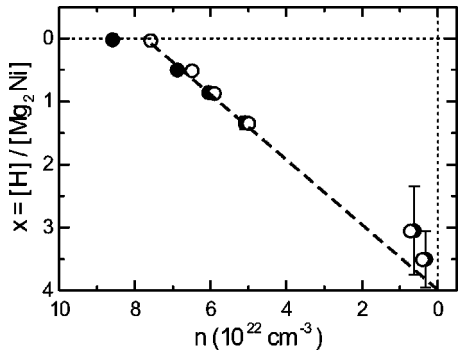

FIG. 6. The six values of the hydrogen concentration x in Mg_2NiH_x ($x=0$, 0.5, 0.7, 1.3, 3.1, and 3.5) determined electrochemically by Lohstroh *et al.*[22] as a function of the charge-carrier density n obtained in this work from Hall-effect measurements at 4.2 K (bullets) and 100 K (open symbols). The straight line $x = 4 - 0.53\times10^{-22}$ cm$^3\times n(x)$ is consistent with the anionic H^- model: each added H atom removes one electron from the conduction band of the host metal.

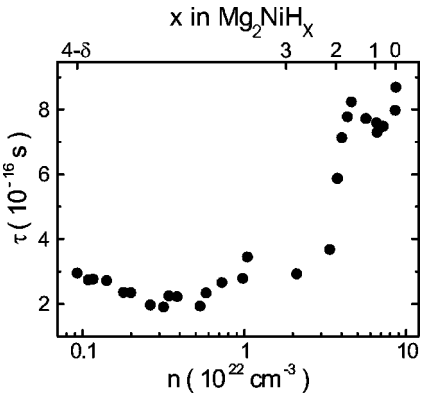

FIG. 7. Scattering time τ as a function of the charge-carrier density n in Mg_2NiH_x ($0<x<4$) at 4.2 K. The upper scale gives x estimated from Eq. (5). Since the stoichiometric limit $x=4$ cannot be shown on the logarithmic scale of n, the highest H concentration $4-\delta$ (i.e., $\delta=0.05$) reached in this work is given.

In Fig. 6, we show the six H concentration x (determined from electrochemical loading experiments as described above) as a function of n (determined from Hall-effect measurements at 4.2 K and 100 K, respectively). Within experimental accuracy, n decreases linearly with x over the entire concentration range (for $0<x<4$), even though Mg_2NiH_x films disproportionate into $Mg_2NiH_{0.3}$ and $Mg_2NiH_{4-\delta}$ phases for $0.3<x<4$.[5] This implies that all the graphs in Figs. 4 and 6 can be regarded as plots as a function of H concentration, with

$$x \simeq 4 - 0.53\times10^{-22}\ \mathrm{cm}^3\times n(x). \tag{5}$$

Equation (5) presents the analytical expression for the anionic H model invoked throughout the present work. Using this relation, an estimate for the H deficiency δ in the $Mg_2NiH_{4-\delta}$ sample with the highest H concentration reached in this work is

$$\delta = (4-x) \simeq 0.53\times10^{-22}\ \mathrm{cm}^3\times n(4-\delta) = (0.049\pm0.005), \tag{6}$$

where $n(4-\delta)=9.27\times10^{20}$ cm^{-3} is the lowest charge-carrier density obtained from Hall-effect data at 4.2 K for $Mg_2NiH_{4-\delta}$. The value of δ (corresponding to $x\simeq3.95$) is small and it indicates that the hydrogenation process at the used pressure of 1.3 bar H_2 was efficient, although incomplete. Higher pressures would be required to reach stoichiometric Mg_2NiH_4 at room temperature.

Within a single-band model, the electrical resistivity is given by

$$\rho=\frac{m^*}{ne^2\tau}, \tag{7}$$

where τ is the *free* charge-carrier relaxation time, m^* the *effective* mass, and e the charge of the electron. On the basis of the experimental data (measured n and ρ) at 4.2 K, we find that τ obtained from Eq. (7) (assuming that $m^*\simeq m_e$, with $m_e\sim9.1\times10^{31}$ kg the mass of the free electron) varies by a factor of ~4 (see Fig. 7).

In the solid-solution limit [$0<x<0.3$, that is, for samples with $\rho(4.2\text{ K})\lesssim60\ \mu\Omega$ cm in Fig. 2], the applicability of the single-band (free electron) model to Mg_2NiH_x is not surprising. In metallic Mg_2Ni, the Fermi energy ϵ_F lies near the $3s$-type Mg band, whose role is that of the conduction band. In dilute Mg_2NiH_x (with $0<x<0.3$), the gradual reduction of n is accompanied by a decrease of ϵ_F within the $3s$-Mg band, whose dispersion is high [its Fermi velocity is large $v_F\simeq10^6$ m/s, typical for light charge carriers (electrons)[24]]. In this regime, τ is essentially constant ($\simeq8.5\times10^{-16}$ s) (see in Fig. 7). The corresponding electron mean free path l_{mfp} ($=\tau v_F$) is $\simeq5$ Å. Such a small value for l_{mfp} ($l_{mfp}<a$, where $a=5.22$ Å is the lattice spacing[6]), indicates that disorder is present at atomic length scale. This is in agreement with the relatively poor crystallinity deduced from x-ray spectra (in as-deposited films) and the low residual resistivity ratio ($\rho_{295\text{ K}}/\rho_{4.2\text{ K}}\sim1.16$) obtained for metallic Mg_2Ni.

At higher H concentrations (see in Fig. 7), τ is no longer constant; i.e., τ drops rapidly by a factor of ~4.5, from 8.5×10^{-16} s in $Mg_2NiH_{\sim1.3}$ to 1.8×10^{-16} s for $Mg_2NiH_{\sim3.5}$. This may be due to percolationlike phenomena assisting the electrical transport in samples with $x>0.3$, resulting from coexistence of metallic $Mg_2NiH_{0.3}$ and semiconducting $Mg_2NiH_{4-\delta}$ phases.[5] In samples with $x\gtrsim3.5$, τ increases slightly.

B. Composite $Mg_2NiH_{0.3}$-$Mg_2NiH_{4-\delta}$ hydrides

Since films of Mg_2NiH_x with $0.3<x<4$ disproportionate, the electrical resistivity and the magnetotransport data presented in this work should be viewed as *effective* transport properties of a composite system, consisting of metallic $Mg_2NiH_{0.3}$ and semiconducting $Mg_2NiH_{4-\delta}$.

We use Bruggeman's effective medium theory[18] to calculate the *effective* electrical resistivity ρ of a binary mixture of $Mg_2NiH_{0.3}$ and $Mg_2NiH_{4-\delta}$,

$$(1-f)\frac{\rho-\rho_S}{\rho+A\rho_S}+f\frac{\rho-\rho_M}{\rho+A\rho_M}=0, \tag{8}$$

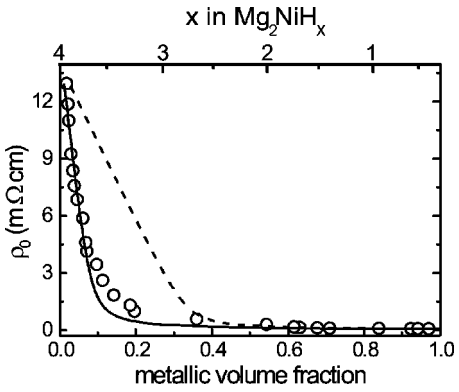

FIG. 8. Electrical resistivity ρ_0 as a function of the metallic volume fraction f in Mg_2NiH_x (with $0.3<x<4$). The continuous and dashed curves are obtained using Eq. (8), and correspond to oblate ($A=11.5$) and spherical ($A=2$) inclusions, respectively. The upper scale gives x estimated from Eq. (5).

where ρ_M is the resistivity of metallic $Mg_2NiH_{0.3}$ and ρ_S that of semiconducting $Mg_2NiH_{4-\delta}$, and f is the volume fraction of the metallic $Mg_2NiH_{0.3}$ phase. The shape of the inclusions in the composite medium is accounted by the geometric factor $A=1/D-1$, where $0<D<1$ is the depolarization factor of the inclusions; i.e., $D=1/3$ for spherical inclusions, while $D>1/3$ and $D<1/3$ correspond to prolate and oblate spheroids, respectively.[25] We consider only spheroids with an axis of rotation perpendicular to the plane of the films since no particular texture has been obtained in our samples.

The metallic volume fraction f can be estimated by using the fact that the partial molar volume of H in metal hydrides is essentially concentration independent.[21] This implies that the volume of Mg_2NiH_x increases linearly with x, i.e., $\varepsilon(x)=\Delta V(x)/V_0=0.08x$ for $0<x<4$. The metallic volume fraction $f=[V(4)-V(x)]/[V(4)-V(0.3)]$ can then be expressed as

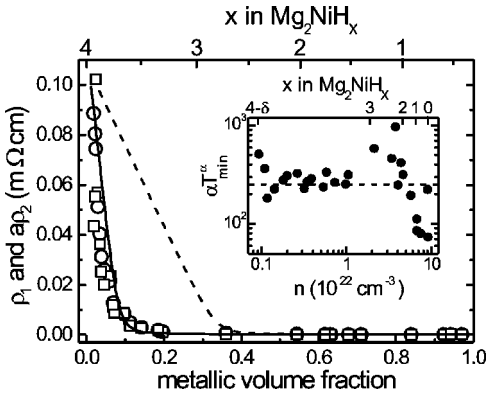

FIG. 9. Kondo ρ_1 (circles) and electron-electron $a\rho_2$ (scaled with $a=250$, squares) amplitudes as a function of the metallic volume fraction f in Mg_2NiH_x (with $0.3<x<4$). The continuous and dashed curves correspond to oblate ($A=11.5$) and spherical ($A=2$) inclusions in Eq. (8), respectively. The inset shows that the values for $\alpha T_{\min}^{\alpha}$ cluster around $\simeq250$. The upper scales give x estimated from Eq. (5). In the inset, since the stoichiometric limit $x=4$ cannot be shown on the logarithmic scale of n, the highest H concentration $x=4-\delta\simeq3.95$ reached in this work is given.

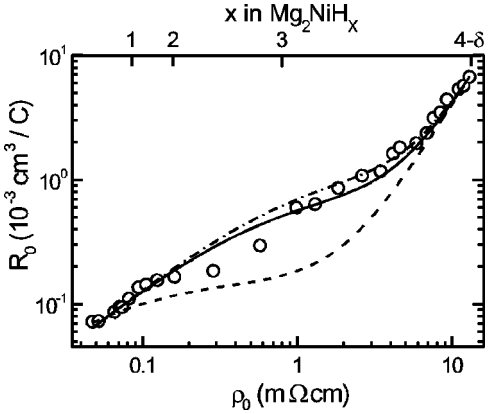

FIG. 10. Measured Hall coefficient R_0 (at 4.2 K) as a function of electrical resistivity ρ_0 in Mg_2NiH_x (for $0.3<x<4$). The continuous and the dashed curves are obtained using Eq. (11), in which $A=11.5$ and 2, respectively. The dotted line is a fit of Eq. (11) to the data using $A=17.7$. The upper scale gives x estimated from Eq. (5). Since the stoichiometric limit $x=4$ cannot be shown on the logarithmic scale of ρ_0, the highest H concentration $4-\delta$ (i.e., $\delta=0.05$) reached in this work is given.

$$f=\frac{4-x}{3.7}=\frac{0.53}{3.7}\times 10^{-22}\ \text{cm}^3\times n(x). \tag{9}$$

The second equality is obtained from Eq. (5), in which the corresponding charge-carrier density $n(x)$ at 4.2 K is used.

We show now that the geometrical factor A can easily be determined from a fit of Eq. (8) to the experimental resistivity data given in Fig. 4(a). For this, we use $\rho_M=\rho_0(x=0.3)\simeq 0.06$ mΩcm and $\rho_S=\rho_0(x\simeq 3.95)=12.94$ mΩcm for the metallic $Mg_2NiH_{0.3}$ and the semiconducting $Mg_2NiH_{4-\delta}$ phases, respectively.

In Fig. 8, ρ_0 is shown as a function of f for two different values of A. The dashed line is for $A=2$, which corresponds to spherical inclusions ($D=1/3$). Clearly, the data are inconsistent with the spherical geometry of the constitutive inclusions. A reasonably good fit is, however, obtained with $A=(11.5\pm 0.5)$ for *all* compositions. The corresponding depolarization factor is $D=1/(A+1)=(0.080\pm 0.003)$. This implies that the inclusions are very flat oblate spheroids, with symmetry axis perpendicular to the plane of the film.

With the same effective medium theory, we discuss now the dependence of the Kondo term ρ_1 and the electron-electron term ρ_2 on f. For that, the explicit temperature dependence of ρ_M, ρ_S, and ρ given by Eq. (3) is taken into account. As both ρ_1 and ρ_2 are related to the temperature dependence of ρ, we calculate $\tilde{\rho}=-\partial\rho(T)/\partial\ln T$ from Eq. (8), assuming that the metallic volume fraction f and the geometrical factor A are temperature independent. This is certainly true at low temperatures. We obtain that

$$(1-f)\frac{\rho\tilde{\rho}_S-\tilde{\rho}\rho_S}{(\rho+A\rho_S)^2}+f\frac{\rho\tilde{\rho}_M-\tilde{\rho}\rho_M}{(\rho+A\rho_M)^2}=0. \tag{10}$$

At low temperatures, $\tilde{\rho}=\rho_1$, while at intermediate temperatures $\tilde{\rho}\approx-\alpha\rho_2 T^{\alpha}$. For $T=T_{\min}$, we have $\tilde{\rho}=\rho_1=\alpha\rho_2 T_{\min}^{\alpha}$ from Eq. (4). In the inset of Fig. 9, we show that the values for $\alpha T_{\min}^{\alpha}$, calculated using the data given in Figs. 4(d) and 4(e), cluster around 250. One expects thus that ρ_1 and, ρ_2 are approximately proportional and, accordingly, that both ρ_1 and ρ_2 satisfy Eq. (10). This is explicitly shown in Fig. 9, where ρ_2 is multiplied by a factor $a\sim 250$ for a direct comparison with ρ_1. The overall features exhibited by ρ_0 (in Fig. 8), ρ_1 and $a\rho_2$ (in Fig. 9) as a function of f are the same. In samples with relatively high H concentration (up to $x\simeq 3.5$), the values for ρ_0, ρ_1, and ρ_2 are low. In samples with $x>3.5$, the values for ρ_0, ρ_1, and ρ_2 diverge with decreasing f (increasing x). Note that the same value $A=11.5$ reproduces nicely the f dependence of ρ_1 and ρ_2. Here again a model assuming spherical inclusions fails completely.

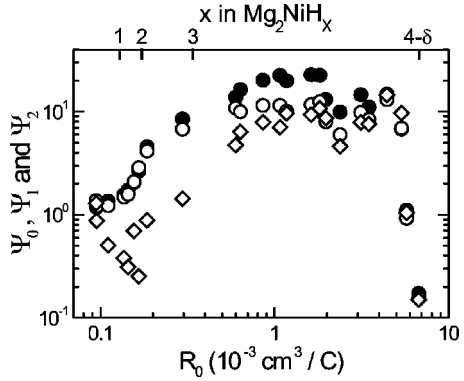

FIG. 11. Variation of Ψ_0, Ψ_1, and Ψ_2 calculated using Eqs. (12) and (13) as a function of the *effective* Hall coefficient R_0 determined experimentally at 4.2 K. The upper scale gives x estimated from Eq. (5). Since the stoichiometric limit $x=4$ cannot be shown on the logarithmic scale of R_0, the highest H concentration $4-\delta$ (i.e., $\delta=0.05$) reached in this work is given.

So far, we have only used electrical resistivity data to determine the geometrical factor A of the inclusions in our composite samples. For this, we needed an explicit relation between f and x. We show now that, using both the electrical resistivity *and* Hall-effect data, A can be determined without any assumption concerning f. For that, we rely on Eq. (A8), derived in the Appendix of this paper, which relates the measured values of the electrical resistivity ρ and Hall coefficient R; i.e.,

$$\frac{R_M\rho^2-R\rho_M^2}{R\rho_S^2-R_S\rho^2}=\frac{\rho-\rho_M}{\rho_S-\rho}\,\frac{\rho+A\rho_M}{\rho+A\rho_S}, \tag{11}$$

where R_M and R_S are, respectively, the measured Hall coefficients of the metallic $Mg_2NiH_{0.3}$ and the semiconducting $Mg_2NiH_{4-\delta}$ phases (including their temperature dependence). The symbols ρ, ρ_M, and ρ_S are the same as before. At 4.2 K, the Hall coefficients in Eq. (11) are $R_{0M}=1/en(x=0.3)=8.64\times 10^{-5}$ cm^3/C for metallic $Mg_2NiH_{0.3}$ and $R_{0S}=1/en(x\simeq 3.95)=6.74\times 10^{-3}$ cm^3/C for semiconducting $Mg_2NiH_{4-\delta}$.

In Fig. 10, the measured Hall coefficients R_0 (i.e., at 4.2 K) are shown as a function of ρ_0. In the same figure, we also

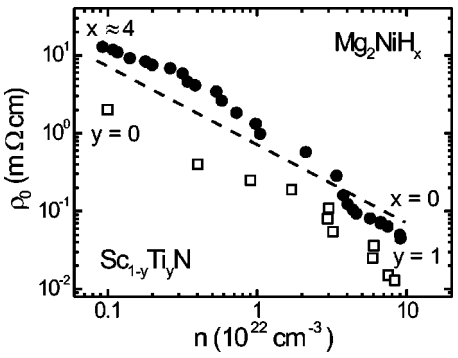

FIG. 12. Electrical resistivity ρ_0 as a function of charge-carrier density n in Mg_2NiH_x hydrides ($0<x<4$) and $Sc_{1-y}Ti_yN$ ($0\leqslant y\leqslant 1$). For Mg_2NiH_x, the data are those at 4.2 K (bullets). The data for $Sc_{1-y}Ti_yN$ are taken from Ref. 19 at 20 K. The dashed line of slope -1 represents the expected dependence of ρ_0 as a function of n in a single-band model, i.e., $\rho_0 \propto 1/n$.

plot R calculated as a function of ρ using Eq. (11), for the values $A=2$ and $A=11.5$, i.e., for spherical (dashed curve) and oblate (continuous curve) inclusions, respectively. The dotted curve is a fit to the data using Eq. (11). The fit yields $A=(17.7\pm 0.7)$, from which $D=(0.053\pm 0.003)$ is obtained. This very low value for D confirms our former conclusion that the inclusions are very flat oblate spheroids.

We demonstrate next that our experimental results can be discussed independently of the metallic volume fraction f and the geometrical factor A of the constitutive inclusions. For that, we rely on Eqs. (A14) and (A15) in the Appendix, which indicate that ρ_0, ρ_1, and ρ_2 can be scaled as a function of measured R_0 only. We define

$$\Psi_i(R_0)=\frac{\rho_i}{\rho_{iM}+k_0\rho_{iS}} \tag{12}$$

with $i=0,1$, and 2. The parameter k_0 defined as

$$k_0=\frac{R_{0M}\rho_0^2-R_0\rho_{0M}^2}{R_0\rho_{0S}^2-R_{0S}\rho_0^2} \tag{13}$$

depends only on the values of measured electrical resistivity and Hall coefficients at a given temperature. In Eq. (12), the values for ρ_0, ρ_1, and ρ_2 are taken from Figs. 4(a)–4(c), respectively. With these, in Fig. 11, Ψ_0, Ψ_1, and Ψ_2 are plotted as a function of R_0 determined from Hall-effect data at 4.2 K. The data for Ψ_0 and Ψ_1 collapse essentially into one curve. A similar R dependence is exhibited by Ψ_2, especially at relatively high H concentrations where the approximation $\rho_1\simeq 250\rho_2$ is better satisfied (see inset in Fig. 9).

It is noteworthy to point out that in Figs. 4(a)–4(c), the electrical resistivity $\rho_0=\rho(T=1\ \mathrm{K})$, the Kondo ρ_1, and electron-electron ρ_2 amplitudes vary over very different ranges; i.e., $10^{-2}<\rho_0(\mathrm{m}\Omega\mathrm{cm})\lesssim 10$, $10^{-5}<\rho_1(\mathrm{m}\Omega\mathrm{cm})\lesssim 10^{-1}$, and $10^{-7}<\rho_2(\mathrm{m}\Omega\mathrm{cm})\lesssim 10^{-3}$. However, with the help of k_0 defined in Eq. (13), ρ_0, ρ_1, and ρ_2 collapse into essentially a single curve as a function of the Hall coefficient R. This can be considered as an *a posteriori* confirmation of the applicability of Bruggeman's effective medium theory to the case of a binary mixture of $Mg_2NiH_{0.3}$ and $Mg_2NiH_{4-\delta}$.

C. Comparison to Sc-Ti-N

The fact that our $Mg_2NiH_{4-\delta}$ films exhibit optical transparency ($E_g=1.6$ eV),[4] although their electrical conductivity and charge-carrier density are high and basically independent of temperature, is not an exception among the variety of materials known nowadays. Recently, Gall *et al.*[19] have shown that, for compositions between $0\leqslant y\leqslant 1$, the electrical and optical properties of $Sc_{1-y}Ti_yN$ alloys can be tuned from semiconducting ScN ($E_g=1.3$ eV) to metallic TiN. For a typical 200 nm $Sc_{1-y}Ti_yN$ film, n at 20 K increases from 1.1×10^{21} cm^{-3} for ScN to 4.6×10^{22} cm^{-3} for TiN. This is accompanied by a decrease of the electrical resistivity ρ_0 (over two orders of magnitude), from 2 mΩcm for ScN to 13 $\mu\Omega$cm for TiN. Quantitatively, these values resemble very much those found in the present work. We emphasize that in Fig. 12, where their ρ_0 and n are represented against each other in log-log scale. For the $Sc_{1-y}Ti_yN$ alloy, the major contribution to the conductivity is the increased carrier concentration n due to substitution of TiN for ScN. In this picture, Gall *et al.* show that each TiN formula unit provides one electron to the conduction band resulting in a metallic resistivity.[19] In our Mg_2NiH_x hydride, this is equivalent to the anionic picture for H in the host lattice: each H atom removes one electron from the conduction band resulting in an increased resistivity. These features are consistent with a single-band model, where the charge-carrier density is reduced gradually upon doping. This corresponds to the straight line of slope -1 in Fig. 12.

Similarly, the optical reflection spectra of black $Mg_2NiH_{0.7}$ (Ref. 15) and $Sc_{0.69}Ti_{0.31}N$ (Ref. 19) measured in films with comparable thickness (200 nm thick), resemble each other. Their reflection is low ($<20\%$) over the entire visible spectrum and exhibits similar features as a function of the photon energy $\hbar\omega$. However, the optical transmission spectra of these films exhibit a completely *different behavior*. Black $Mg_2NiH_{0.7}$ films are essentially nontransparent; i.e., their transmission is extremely small ($<0.01\%$) over the entire visible spectrum [$0.75<\hbar\omega$ (eV) <3.50]. $Sc_{0.69}Ti_{0.31}N$ films, on the contrary, exhibit a transparent window around $\hbar\omega\simeq 2.1$ eV, corresponding to the photon energy at which the reflection is minimum. The optical transmission is as large as $\sim 8\%$. Using a Drude-Lorentz model, the optical transmission and reflection spectra in $Sc_{0.69}Ti_{0.31}N$ can be fitted simultaneously. In black $Mg_2NiH_{0.7}$, simultaneous fits to the optical transmission and reflection spectra are not possible. In *all* these fits, the parameters obtained reproduce some optical transmission ($\sim 10\%$) at $\hbar\omega\simeq 1.24$ eV, where the reflection exhibits a minimum ($\simeq 5\%$) (see in Ref. 15). These features suggest that the simultaneous occurrence of a low reflection ($<15\%$) and a very low transmission ($<0.01\%$) in black $Mg_2NiH_{0.7}$ films is related to the very flat oblate spheroidal inclusions in our composite. This is discussed in detail elsewhere.[22]

V. CONCLUSIONS

We have investigated the temperature (between 2 K and 280 K) and concentration (for $0<x<4$) dependencies of the electrical resistivity, charge-carrier density, and magnetoresistance of Mg_2NiH_x switchable mirrors. Although ρ increases by almost three orders of magnitude upon transition from metallic Mg_2Ni to transparent $Mg_2NiH_{4-\delta}$, n decreases gradually from typically 10^{23} cm^{-3} to 10^{21} cm^{-3}. These metallic features indicate that $Mg_2NiH_{4-\delta}$ prepared at room temperature under 1300 mbar H_2 is a heavily doped semiconductor. The estimated nonstoichiometry δ is ~ 0.05.

By combining Hall-effect, electrical resistivity, and electrochemical data, we showed that $n \propto (4-x)$, which confirms that the role played by hydrogen in the host lattice is that of a negatively charged H^- ion. Our data indicate that, in the limit $\delta \to 0$, Mg_2NiH_4 is a semiconductor. This is in agreement with the electronic ground state of LT-Mg_2NiH_4 found by Myers *et al.*[12]

At all concentrations (between $0<x<4$), the temperature dependence of the electrical resistivity is well described by $\rho(T)=\rho_0-\rho_1 \ln T+\rho_2 T^{1.85}$. The $\ln T$ dependence below 10 K is due to Kondo effect. Between 25 K and 80 K, $\rho(T)$ is dominated by electron-electron scattering effects. The scattering amplitudes ρ_0, ρ_1, and ρ_2 exhibit similar dependencies as a function of n, i.e., power-law behavior over two orders of magnitude of n. These dependencies are well described within an effective medium theory, where Mg_2NiH_x $(0.3<x<4)$ disproportionates into metallic $Mg_2NiH_{0.3}$ and semiconducting $Mg_2NiH_{4-\delta}$. The electrical and magnetotransport data at 4.2 K are consistent with the oblate geometry of the metallic $Mg_2NiH_{0.3}$ inclusions. In the same framework, we show that, independently of the geometry and the volume fraction of the metallic inclusions, the scattering amplitudes ρ_0, ρ_1, and ρ_2 in $\rho(T)$ can be scaled as a function of $R=1/ne$. This is remarkable, since these scattering amplitudes describe very different physics.

Concerning the highly absorbing state in $Mg_2NiH_{0.7}$ samples, we have found that n (at 4.2 K) is reduced only by a factor ~ 1.43 with respect to that in metallic Mg_2Ni. This implies that the black state in $Mg_2NiH_{0.7}$ cannot be explained by a dramatic reduction of n (by a factor 25), as previously suggested in Ref. 15. A hint to understanding the occurrence of the black state may be the peculiar geometry of the metallic inclusions (i.e., very flat oblate spheroids) found in composite $Mg_2NiH_{0.3}$-$Mg_2NiH_{4-\delta}$ films, which is also responsible for the metallic features (e.g, low electrical resistivity) exhibited in samples with relatively high H content ($x \simeq 3.5$). The film is to a large extent electrically shunted by the flat metallic spheroids.

The electrical and magnetotransport properties of Mg_2NiH_x films $(0<x<4)$ resemble those of $Sc_{1-y}Ti_yN$ alloys $(0 \leqslant y \leqslant 1)$, which also switch from metallic (ScN) to semiconducting (TiN). In these systems, the electrical resistivity and the charge-carrier density can be described with a simple electronic band model in which the roles played by H (in Mg_2NiH_x) and Ti (in $Sc_{1-y}Ti_yN$) are similar: each H atom removes one electron from the Mg_2Ni host metal, while in $Sc_{1-y}Ti_yN$ alloys, each Ti provides one extra electron. Both systems exhibit a metal-to-semiconductor transition. However, this transition is much simpler amenable to experimental investigation in Mg_2NiH_x than in $Sc_{1-y}Ti_yN$, since the H concentration can be easily and reversibly varied at will by changing the pressure of the surrounding hydrogen gas, while an entirely new sample has to be made for each composition of $Sc_{1-y}Ti_yN$. In spite of the similarities of their electrical properties, Mg_2NiH_x and $Sc_{1-y}Ti_yN$ have significantly different optical properties: although $Sc_{0.69}Ti_{0.31}N$ and $Mg_2NiH_{0.7}$ have low reflectivities, $Sc_{0.69}Ti_{0.31}N$ has a relatively large transparency window around 2.1 eV while the transmission of $Mg_2NiH_{0.7}$ is vanishingly small (smaller than 0.01%.

ACKNOWLEDGMENTS

The authors thank J. Isidorsson for the sample preparation and RBS analyses, I. A. M. E. Giebels and B. Dam for fruitful discussions, and A. Hoekstra for valuable suggestions. This work was part of the research program of the Stichting voor Fundamenteel Onderzoek der Materie (FOM), financially supported by the Nederlandse Organisatie voor Wetenschappelijk Onderzoek (NWO).

APPENDIX: EFFECTIVE HALL COEFFICIENT FOR A COMPOSITE MEDIUM WITH SPHEROIDAL INCLUSIONS

For the analysis of our experimental data we need explicit relations for the effective electrical resistivity ρ and the Hall coefficient R of a composite medium consisting of metallic and semiconducting inclusions.

For a composite media with *spherical* inclusions, Cohen and Jortner[26] have derived the following implicit expressions for the effective Hall coefficient R:

$$R = HR_M, \tag{A1a}$$

$$\mu = G\mu_M, \tag{A1b}$$

$$H = G/F, \tag{A1c}$$

$$G = \frac{1}{F}\left[1 - \frac{(2F+1)^2(1-f)(1-XY)}{(2F+1)^2(1-f)+(2F+X)^2 f}\right], \tag{A1d}$$

$$Y = \mu_S/\mu_M, \tag{A1e}$$

in which the terms indexed by S and M refer to their values in metallic and semiconducting samples, respectively; $\mu = R\sigma$ is the effective Hall mobility, and f and $(1-f)$ the metallic and semiconducting volume fractions, respectively. In Eq. (A1d), $X=\sigma_S/\sigma_M$. F in Eqs. (A1c) and (A1d) can be obtained as a function of the *effective* electrical conductivity σ and the metallic volume fraction f, using the following system of equations:

$$\sigma = F\sigma_M, \tag{A2a}$$

$$F = a + [a^2 + \tfrac{1}{2}X]^{1/2}, \tag{A2b}$$

$$a=\tfrac{1}{2}[(\tfrac{3}{2}f-\tfrac{1}{2})(1-X)+\tfrac{1}{2}X], \tag{A2c}$$

$$X=\sigma_S/\sigma_M, \tag{A2d}$$

which can be put in a compact formula, similar to that in Eq. (8) (see in Sec. IV B) with $A=2$ (i.e., for *spherical* inclusions). For that purpose, one needs to calculate $(1-f)/f$. From Eqs. (A2b) and (A2c), we obtain

$$f=\frac{1}{3}\frac{F-X}{1-X}\frac{1+2F}{F}. \tag{A3}$$

Using Eq. (A3), after expressing F and X in terms of $\sigma_{M,S}$ and σ using Eqs. (A2a) and (A2d), we obtain

$$(1-f)\frac{\sigma-\sigma_S}{\sigma_S+2\sigma}+f\frac{\sigma-\sigma_M}{\sigma_M+2\sigma}=0, \tag{A4a}$$

which in terms of $\rho=1/\sigma$ is

$$(1-f)\frac{\rho-\rho_S}{\rho+2\rho_S}+f\frac{\rho-\rho_M}{\rho+2\rho_M}=0. \tag{A4b}$$

Equation (A4b) is a special case, corresponding to $A=2$ in Eq. (8) in Sec. IV B.

Equations (A1a)–(A1d) can be put in a compact form, similar to that in Eq. (A4a). First, we use Eq. (A1d) to obtain

$$\frac{1-f}{f}=\frac{1-FG}{(2F+1)^2}\frac{(2F+X)^2}{FG-XY}. \tag{A5}$$

Using Eqs. (A1b) and (A2a), it follows that $FG=\sigma\mu/\sigma_M\mu_M=R\sigma^2/R_M\sigma_M^2$, since $\mu=R\sigma$ and $\mu_M=R_M\sigma_M$ are Hall mobilities. Similarly, we obtain $XY=\sigma_S\mu_S/\sigma_M\mu_M=R_S\sigma_S^2/R_M\sigma_M^2$ using Eqs. (A1e) and (A2d). With these in Eq. (A5) and additionally, expressing F and X in terms of $\sigma_{M,S}$ and σ using Eqs. (A2a) and (A2d), we obtain

$$(1-f)\frac{R\sigma^2-R_S\sigma_S^2}{(\sigma_S+2\sigma)^2}+f\frac{R\sigma^2-R_M\sigma_M^2}{(\sigma_M+2\sigma)^2}=0. \tag{A6}$$

Equation (A6) is Bruggeman's equation for the *effective* Hall coefficient R in a composite medium with *spherical* inclusions, in which σ is the *effective* electrical conductivity given in Eq. (A4a).

To generalize Eq. (A6) to the case of spheroidal inclusions (i.e., *oblate* and *prolate* inclusions with a rotation axis perpendicular to the film's plane), we replace the factor 2 in Eq. (A6) by the geometrical factor A. After substituting σ for $1/\rho$, we obtain

$$(1-f)\frac{R\rho_S^2-R_S\rho^2}{(\rho+A\rho_S)^2}+f\frac{R\rho_M^2-R_M\rho^2}{(\rho+A\rho_M)^2}=0. \tag{A7}$$

Equation (A7) presents the generalized Bruggeman's equation for the *effective* Hall coefficient R as a function of the *effective* electrical resistivity ρ and the metallic volume fraction f of composite media with *spheroidal* inclusions (i.e., with $A=2$ for spherical, $A>2$ for oblate, and $0<A<2$ for prolate inclusions).

Using Eqs. (A4b) and (A7), f can be eliminated to give

$$\frac{R_M\rho^2-R\rho_M^2}{R\rho_S^2-R_S\rho^2}=\frac{\rho-\rho_M}{\rho_S-\rho}\frac{\rho+A\rho_M}{\rho+A\rho_S}. \tag{A8}$$

Except for A, this equation involves only quantities measured at a chosen temperature (e.g., at 4.2 K). Consequently it can be used to determine the geometrical factor A of the constitutive inclusions.

We show now that a relation independent of A can be derived if, besides the data for ρ and R at a given temperature, one uses also data on the temperature dependence of the electrical resistivity ρ. For this, we take the derivative $\partial/\partial\ln T$ of Eq. (A4b) assuming that f and A are temperature independent. We obtain

$$(1-f)\frac{\rho\tilde{\rho}_S-\tilde{\rho}\rho_S}{(\rho+A\rho_S)^2}+f\frac{\rho\tilde{\rho}_M-\tilde{\rho}\rho_M}{(\rho+A\rho_M)^2}=0 \tag{A9}$$

with

$$\tilde{\rho}=-\partial\rho(T)/\partial\ln T. \tag{A10}$$

Using Eqs. (A7) and (A9), we eliminate f to obtain

$$\frac{\tilde{\rho}\rho_M-\rho\tilde{\rho}_M}{\rho\tilde{\rho}_S-\tilde{\rho}\rho_S}=\frac{R_M\rho^2-R\rho_M^2}{R\rho_S^2-R_S\rho^2}. \tag{A11}$$

This equation can be cast in an elegant form by defining

$$k=\frac{R_M\rho^2-R\rho_M^2}{R\rho_S^2-R_S\rho^2}. \tag{A12}$$

Then

$$\frac{\rho}{\rho_M+k\rho_S}=\frac{\tilde{\rho}}{\tilde{\rho}_M+k\tilde{\rho}_S}. \tag{A13}$$

Since at low temperatures $\tilde{\rho}=\rho_1$ and $\rho\simeq\rho_0$ [see Eq. (3) in Sec. II], this relation implies that at a given temperature T_0 (in Sec. IV B, $T_0=1$ K)

$$\Psi_0=\frac{\rho_0}{\rho_{0M}+k_0\rho_{0S}}=\frac{\rho_1}{\rho_{1M}+k_0\rho_{1S}}=\Psi_1. \tag{A14}$$

As furthermore $\rho_1=\rho_2\alpha T_{\min}^{\alpha}\approx 250\rho_2$ [see Eq. (4) in Sec. II], we have

$$\Psi_2=\frac{\rho_2}{\rho_{2M}+k_0\rho_{2S}}\approx\Psi_1. \tag{A15}$$

To clarify the physical meaning of the dimensionless parameter Ψ, we note first that

$$k=\frac{\rho-\rho_M}{\rho_S-\rho}\frac{\rho+A\rho_M}{\rho+A\rho_S}. \tag{A16}$$

We consider now two particular cases of the geometrical factor A. In the limit $A \to \infty$ (i.e., $D \to 0$), the generalized equation of Bruggeman [see Eq. (8) in Sec. IV B] becomes

$$\frac{1}{\rho} = \frac{f}{\rho_M} + \frac{1-f}{\rho_S} \tag{A17}$$

which is in fact the electrical resistivity of a layered system, consisting of metallic and semiconducting sheets of electrical resistivity ρ_M and ρ_S. In this geometry, the metallic volume fraction is $f = d_M/(d_M + d_S)$, where d_M and d_S are the thicknesses of the metallic and semiconducting layers. For $A \to \infty$ in Eq. (A16), we obtain also that

$$k = \frac{\rho - \rho_M}{\rho_S - \rho} \frac{\rho_M}{\rho_S} = \left(\frac{1}{f} - 1\right)\left(\frac{\rho_M}{\rho_S}\right)^2 \tag{A18}$$

and

$$\Psi = \frac{1}{f} \frac{1}{\left(1 + \frac{1-f}{f} \frac{\rho_M}{\rho_S}\right)^2}. \tag{A19}$$

As $\rho_M/\rho_S \ll 1$ (i.e., in our case, $\rho_M/\rho_S \simeq 10^{-3}$), one obtains

$$\Psi \simeq \frac{1}{f} \tag{A20}$$

and Ψ is essentially the *inverse* metallic volume fraction f except for very small $f \ll \rho_M/\rho_S$.

In the limit $A \to 0$ (i.e., $D \to \infty$), the generalized equation of Bruggeman is simply

$$\rho = f\rho_M + (1-f)\rho_S. \tag{A21}$$

Similarly, one finds

$$k = \frac{\rho - \rho_M}{\rho_S - \rho} = \frac{1}{f} - 1 \tag{A22}$$

and

$$\Psi = f. \tag{A23}$$

Thus, in a system consisting of alternating metallic and semiconducting sheets connected in series, Ψ represents the metallic volume fraction f.

[1] J.N. Huiberts, R. Griessen, J.H. Rector, R.J. Wijngaarden, J.P. Dekker, D.G. de Groot, and N.J. Koeman, Nature (London) **380**, 231 (1996).

[2] P. van der Sluis, M. Ouwerkerk, and P.A. Duine, Appl. Phys. Lett. **70**, 3356 (1997).

[3] A.T.M. van Gogh, D.G. Nagengast, E.S. Kooij, N.J. Koeman, J.H. Rector, and R. Griessen, Phys. Rev. B **63**, 195105 (2001).

[4] T.J. Richardson, J.L. Slack, R.D. Armitage, R. Kostecki, B. Farangis, and M.D. Rubin, Appl. Phys. Lett. **78**, 3047 (2001).

[5] J.J. Reilly and R.H. Wiswall, Inorg. Chem. **7**, 2254 (1968).

[6] J. Schefer, P. Fischer, F. Stucki, L. Schlapbach, J.J. Didisheim, K. Yvon, A.F. Andresen, and W. Halg, J. Less-Common Met. **74**, 65 (1980).

[7] Z. Gavra, M.H. Mintz, G. Kimmel, and Z. Hadari, Inorg. Chem. **18**, 3595 (1986).

[8] P. Zolliker, K. Yvon, J.D. Jorgensen, and F.J. Rotella, Inorg. Chem. **25**, 3590 (1986).

[9] B. Darriet, J.L. Soubeyroux, M. Pezat, and D. Fruchart, J. Less-Common Met. **103**, 153 (1984).

[10] D. Noreus and L.G. Olsson, J. Chem. Phys. **78**, 2419 (1983).

[11] G.N. Garcia, J.P. Abriata, and J.O. Sofo, Phys. Rev. B **59**, 11 746 (1999).

[12] W.R. Myers, T.J. Richardson, L.-W. Wang, and M.D. Rubin, J. Appl. Phys. **91**, 4879 (2002).

[13] Z. Gavra, G. Kimmel, Y. Gefen, and M.H. Mintz, J. Appl. Phys. **57**, 4548 (1985).

[14] H. Blomqvist and D. Noreus, J. Appl. Phys. **91**, 5141 (2002).

[15] J. Isidorsson, I.A.M.E. Giebels, M. Di Vece, and R. Griessen, Appl. Phys. Lett. **80**, 2305 (2002).

[16] J. Kondo, Prog. Theor. Phys. **32**, 37 (1964).

[17] W.G. Baber, Proc. R. Soc. London, Ser. A **158**, 383 (1973).

[18] D.A.G. Bruggeman, Ann. Phys. (Leipzig) **24**, 636 (1935); .R. Landauer, J. Appl. Phys. **23**, 779 (1952); .D.S. McLachlan, J. Phys. C **20**, 865 (1987).

[19] D. Gall, I. Petrov, and J.E. Greene, J. Appl. Phys. **89**, 401 (2001).

[20] L.J. van der Pauw, Philips Res. Rep. **13**, 1 (1958).

[21] Y. Fukai, *The Metal-Hydrogen System: Basic Bulk Properties*, Material Science, Vol. 21 (Springer, Berlin, 1993).

[22] W. Lohstroh, R.J. Westerwaal, B. Noheda, S. Enache, I.A.M.E. Giebels, B. Dam, and R. Griessen (unpublished).

[23] N.F. Mott, *Metal-Insulator Transitions* (Taylor & Francis, London, 1990).

[24] C. Kittel, *Introduction to Solid State Physics* (Wiley, New York, 1996).

[25] L.D. Landau and E.M. Lifschitz, *Electrodynamics of Continuous Media* (Pergamon Press, Oxford, 1984).

[26] M.H. Cohen and J. Jortner, Phys. Rev. Lett. **30**, 696 (1973).